Applied Physics Letters

Deterministic modeling of hybrid nonlinear effects in epsilon-near-zero thin films

Cite as: Appl. Phys. Lett. **120**, 031103 (2022); https://doi.org/10.1063/5.0077116
Submitted: 30 October 2021 • Accepted: 15 December 2021 • Published Online: 18 January 2022

R. Secondo, A. Ball, B. Diroll, et al.

AIP Publishing

Applied Physics Letters ARTICLE scitation.org/journal/apl

Deterministic modeling of hybrid nonlinear effects in epsilon-near-zero thin films

Cite as: Appl. Phys. Lett. **120**, 031103 (2022); doi: 10.1063/5.0077116
Submitted: 30 October 2021 · Accepted: 15 December 2021 ·
Published Online: 18 January 2022

R. Secondo,[1] A. Ball,[1] B. Diroll,[2] D. Fomra,[1] K. Ding,[1] V. Avrutin,[1] Ü. Özgür,[1] D. O. Demchenko,[3] J. B. Khurgin,[4] and N. Kinsey[1,a)]

AFFILIATIONS

[1]Department of Electrical and Computer Engineering, Virginia Commonwealth University, Richmond, Virginia 23284, USA
[2]Center for Nanoscale Materials, Argonne National Laboratory, 9700 S. Cass Avenue, Lemont, Illinois 60439, USA
[3]Department of Physics, Virginia Commonwealth University, Richmond, Virginia 23284, USA
[4]Department of Electrical and Computer Engineering, Johns Hopkins University, Baltimore, Maryland 21218, USA

Note: This paper is part of the APL Special Collection on Zero-index Metamaterials for Classical and Quantum Light.
[a)]**Author to whom correspondence should be addressed:** nkinsey@vcu.edu

ABSTRACT

In nonlinear optics, significant effort is concentrated on improving the strength and efficiency of interactions; however, experimentally investigating nonlinear materials is a complex, time-consuming, and costly investment. Moreover, it is often challenging to isolate, study, and optimize material parameters in an experiment due to complexities in the growth process. Recently, epsilon-near-zero materials have received a great deal of attention as promising nonlinear optical materials, but like many up-and-coming materials, the ability to explore and optimize their properties has been challenging. Here, we establish a framework to rapidly evaluate the performance of nonlinear epsilon-near-zero materials for both inter- and intraband effects *in silico*, requiring only an energy–momentum (E–*k*) diagram, linear optical properties, and experimental conditions. Measured nonlinear reflection and transmission in gallium-doped zinc oxide films are compared to the numerical framework for both intra- and interband excitation to verify accuracy across wavelength and irradiance while two figures of merit (FoMs) are introduced to quickly evaluate the performance of films without a full numerical framework. This capability is used to predict the performance of highly doped gallium nitride, cadmium oxide, zinc oxide, and indium tin oxide films, and efficient intra- and interband operation conditions are identified. Through this numerical framework and the FoMs, the exploration of unstudied epsilon-near-zero materials is enabled without the need for a nonlinear experiment, thereby accelerating the search for more efficient nonlinear materials and excitation conditions.

Nonlinear optics is well-known to be limited by the weak interaction of light and matter, which has fostered research into improved materials for ultrafast on-chip and interactions.[1] Recent research has explored organic materials,[2,3] 2D materials,[4,5] and metamaterials[6–9] as well as emerging topological structures[10,11] to improve nonlinear effects. Among them, epsilon-near-zero (ENZ)[12–26] materials—films with a condition of $Re\{\varepsilon\} = 0$—have received significant attention.[12,13] Recent experiments have shown large modulation of reflection-transmission[17,27,28] as well as adiabatic frequency conversion[29,30] driven by a strong intensity-dependent refractive index (IDRI). Such enhanced nonlinearities arise due to the inherent features of ENZ, which combine a "slow," but fast enough (∼THz scale), free-carrier nonlinearity that enables interactions to accumulate over the pulse width alongside slow light enhancement and strong field localization.[12,29,31] It is also important to note the distinction between the ENZ and near-zero-index (NZI). Both ENZ and NZI conditions can be achieved in homogeneous materials (e.g., doped films or phononic materials), which achieve local ENZ/NZI conditions.[17,32,33] On the other hand, structured materials (e.g., metamaterials or waveguides) achieve an effective or macroscopic "near-zero-wavevector" condition through geometric manipulation of finite permittivity constituents.[6–9,35,36] While both approaches can be useful in their own right, the enhancements provided to nonlinear phenomena differ. Researchers should consider the end goals when making use of ENZ enhancement.[12,13] Here, we focus our efforts on the study of degenerately doped semiconductors as they provide ENZ properties without requiring complex nanofabrication while offering all nonlinear enhancement mechanisms.

A large IDRI has been experimentally shown in several homogeneous ENZ materials, including transparent conducting oxides (TCOs) at near-infrared wavelengths.[33,34] The genesis of the large IDRI of TCOs stems from the redistribution of free electrons in the E–k space and their resulting occupation of states with differing effective masses (intraband) as well as the generation of additional electron-hole pairs within the material (interband).[12,28,37] A non-parabolicity parameter can be invoked to describe this response,[38–42] but this approach generally requires the non-parabolicity parameter to be known *a priori*, limiting the applicability to well-established materials.

In this work, we aim to establish a closed-loop predictive framework for evaluating both the interband and intraband nonlinear response of ENZ materials using a kinetic model. Our approach is verified using nonlinear reflection measurements on Ga:ZnO and then expanded to materials XX:GaN and YY:CdO (XX is Ge[43,44] or Si[45] and YY is Dy,[46] F,[47] or In[48]), requiring only the input of a band structure and relevant experimental parameters. Calculations are performed for both interband and intraband nonlinear processes of films within current doping limits or just beyond, and a figure of merit (FoM) for each effect is outlined. The model provides a feasible way to change material properties that are typically controlled by growth conditions to highlight performance tradeoffs and rapid material evaluation.[14]

For refractive index nonlinearities in homogeneous ENZ materials, two potential processes are possible: intraband transitions that redistribute the electrons in the E–k space and interband transitions that produce excess free carriers.[28,37] In the case of intraband processes, absorption results in excess energy density stored in the material

$$\Delta U_{IR}(t) = A(\lambda_{IR}, t)\frac{I_{0IR}t_{IR}}{d}\eta_{IR}(t), \tag{1}$$

where $A(\lambda_{IR}, t)$ is the absorptivity at the IR pump wavelength calculated through the angularly resolved transfer matrix method.[49] I_{0IR} is the incident IR pump intensity, t_{IR} is the pump pulse FWHM, d is the film thickness, and $\eta_{IR}(t)$ is the fraction of energy in the material from the pump given by

$$\eta(t) = \frac{1}{2}\left(\mathrm{erf}\left(\frac{t}{\sigma}\right)+1\right)\begin{cases}1, & t<0,\\ e^{-\frac{t}{\tau_{IR}}}, & t\geq 0,\end{cases} \tag{2}$$

where σ is the time of the Gaussian IR pump pulse. After thermalization of the non-equilibrium electron population through electron–electron scattering (occurring on the order of 10s fs[47,48]), the absorbed energy causes a rise in the effective electron temperature, T_e, inducing high energy or "hot" electrons that are heavier than their low energy counterparts. This energy relaxes to the lattice through electron–phonon scattering with a characteristic time of τ_{IR}, generally been shown to be ∼200 fs.[50,51]

As the excited electrons remain at higher energies in the band, the average effective mass of the electrons increases, calculated for any temperature, T_e and carrier concentration, N, through

$$m^*_{avg}(T_e) = \left(\frac{1}{N}\int_0^\infty \frac{f(\mu, T_e, E)\rho(E)}{m^*(E)}dE\right)^{-1}, \tag{3}$$

where $f(\mu, T_e, E)$ is the Fermi–Dirac distribution of carriers with a chemical potential μ, $\rho(E)$ is the density of states (DOS) of the conduction band near the Γ point, and $N = \int_0^\infty f(\mu, T_e, \rho(E)dE$. The optical effective mass as a function of energy is calculated through[16]

$$m^*(E) = \left(\frac{2}{3\hbar^2 k}\frac{dE}{dk} + \frac{1}{3\hbar^2}\frac{d^2E}{dk^2}\right)^{-1}. \tag{4}$$

Inherent to this assumption is that the conduction band minimum (CBM) is located at the Γ point, exhibits spherical symmetry, and is not degenerate at Γ. Materials such as GaN, CdO, ITO, and AZO all fit these conditions while other well-known films, such as Si, require tensor nature and the consideration of multiple valleys.

In the case of interband processes, absorption results in the production of excess electrons with density

$$\Delta N = A(\lambda_{UV}, t)\frac{I_{0UV}t_{UV}}{d}\frac{1}{\hbar\omega}\eta_{UV}(t), \tag{5}$$

where η_{UV} is given in Eq. (2) replacing τ_{UV} for the relaxation time of the interband process. As free carriers are generated, an equal density of holes is also generated in the valence band forming an e–h pair. The optical contribution of the generated holes can be neglected for many materials due to their high effective mass, which only slightly alters the conductivity.[52] The relaxation rate for the e–h pairs varies greatly based on material quality and doping levels between 100s of femtoseconds and the picoseconds. The increase in the carrier concentration from interband absorption also induces an increase in energy of the electron sea to account for the new carriers. This change in the energy density is approximated as

$$\Delta U_{UV} \approx \Delta N\left(\mu + \frac{\Delta N}{\rho(\mu)}\right), \tag{6}$$

where $\Delta N/\rho(\mu)$ is approximately the change in the Fermi level.

Following these calculations, two conservation equations can be established to encompass both effects—conservation of carriers and conservation of energy

$$N = N_0 + \Delta N = \int_0^\infty f(\mu, T_e, E)\rho(E)dE, \tag{7}$$

$$U = U_0 + \Delta U_{IR} + \Delta U_{UV} = \int_0^\infty f(\mu, T_e, E)\rho(E)EdE, \tag{8}$$

where U_o is the linear energy density of the system. By solving these equations in tandem, μ and T_e can be calculated at every point in time for any combination of UV and IR pumps. This allows calculation of m^*_{avg} and, thus, the permittivity as described through the Drude model.

For simplicity, we consider films thin enough to assume the absorption is uniformly distributed throughout the film ($d < 1/\alpha$), but note that the model can be extended to include thickness dependence. This is a good assumption for common ENZ materials such as ITO and Al:ZnO studied in the literature[27,32,33,53] with film thicknesses ∼300 nm. This assumption holds true for interband as long as the UV pump is at the band edge. Additionally, the permittivity change attributed to Moss–Burnstein shifts is not considered, and the bandgap is fixed, allowing a single ε_∞ in the near-infrared to account for high-frequency absorption. This is a reasonable assumption for low to moderate pumping regimes but would lead to deviations under high UV pump irradiances as band filling would result in saturation of the UV pump absorption.

To verify the model, nonlinear reflection measurements were conducted on a GZO film with ENZ $\varepsilon(\lambda_{ENZ} = 1700\,\text{nm}) = 0 + i0.41$ and a thickness of 225 nm grown on 24 nm of ZnO on a c-plane sapphire substrate.[54–56] Linear optical properties were determined via variable angle spectroscopic ellipsometry (J.A. Woollam M-2000),[57] performing successive measurements of the sapphire substrate, ZnO/sapphire, and finally, GZO/ZnO/sapphire to ensure accurate extraction. Nonlinear pump-probe experiments were conducted for both a near-infrared pump at 1890 nm (to excite an intraband effect) and an ultraviolet pump at 325 nm (to excite an interband effect), each with a 60 fs pulse width, see Fig. 1(a). A white light probe is generated from the pump by focusing the beam inside a 5 mm thick sapphire crystal and is used to observe the change in the sample's reflection and transmission over the range of 1150–1600 nm using a pair of CCDs (Ultrafast Systems Cam NIR-2). The pump pulse is chopped at 2.5 kHz with a laser repetition rate of 5 kHz. The white light probe ($<10°$ with respect to pump angle) was detected at 5 kHz, therefore directly measuring the difference between the pumped and unpumped samples to generate $\Delta R/R$. Reflection data were taken at 30° from the sample normal. In all cases, the pump was horizontally polarized while the probe was vertically polarized and in the same plane to minimize two-beam coupling effects.[58] The peak irradiance of the IR pump at 1890 nm was 13, 33, and 83 GW/cm^2 ($P_{avg} = 1.3$, 3.3, and 8.3 mW, respectively) and 1, 2, 6, and 14 GW/cm^2 ($P_{avg} = 0.2$, 0.5, 1.3, and 3.1 mW, respectively) for the UV pump at 325 nm with results shown in Figs. 2(a)–2(d). These intensities are below the damage threshold for GZO.[28]

To fit the experimental data, theoretical E–k diagrams for ZnO were computed using the Heyd–Scuseria–Ernzerhof (HSE) hybrid density functional theory[59] as implemented in VASP code,[60] tuned to reproduce the experimental bandgap of each material, see Fig. 1(b). Plane-wave energy cutoffs of 500 eV were used in all cases. The experimental lattice structure is taken as a starting point, and the fraction of exact exchange α and the range separation parameter μ are adjusted to yield the low-temperature experimental bandgap at the Γ-point, resulting in $\alpha = 0.3$ and $\mu = 0.0517$ 1/Å for ZnO. The lattice structure is then relaxed using the bandgap-tuned HSE to within 0.01 eV/Å, and the band structure is calculated. The lattice relaxations result in a slight deviation from the experimental bandgap; however, tests show that effective masses are only weakly affected by the slight differences between experimental and theoretical band gaps.[61] The conduction band of Ga:ZnO was obtained from ZnO assuming the band is filled with electrons according to the Fermi–Dirac distribution, and assuming the bandgap renormalization effects are negligible.

Taking the E–k diagram of Ga:ZnO, shown in Fig. 1(b), as well as the experimental parameters, the theory can predict the peak magnitude of the change in reflection vs irradiance and probe wavelength for both inter- and intraband nonlinear effects without fitting parameters, see Figs. 2(c) and 2(d). Variations between the predicted linear reflection of the sample and the reflection as measured through FTIR account for some errors in the spectral location of the theoretical curves compared to measured results, particularly in the short wavelength region of Fig. 2(c). When observing the results, we note the change in sign of the normalized reflection in both pumping scenarios. The refractive index of our film is less than unity for the majority of wavelengths, wherein excitation can be thought of as moving the material closer to an impedance matching condition with air (intraband) or becoming further mismatched (interband). However, for short wavelengths, the linear impedance of GZO is already close to that of air, and thus, at shorter wavelengths, the behavior is reversed.

By establishing the validity of the model, we can then extend the framework to additional materials and rapidly evaluate their performance as nonlinear ENZ materials for both inter- and intraband effects *in silico*, requiring only an E–k diagram, linear optical properties, and experimental conditions. In particular, the popular ENZ films ZnO heavily doped with Ga or Al (GZO and AZO, respectively) and ITO are evaluated alongside heavily doped CdO and GaN for three values of ε'' at the permittivity crossover and several intensities of inter- and intraband pumping, see Figs. 3(a)–3(d). The linear properties of each material used for the calculations are listed in Table I, and the HSE hybrid density functional theory parameters of the gap tuned materials are shown in Table II.

To decode the effects further and enable rapid evaluation of other materials without the full numerical framework, a FoM can be established for both effects. In our previous work, an intraband FoM is developed as[16]

$$FoM_{intra} = A_{pump}\left[\frac{1}{m^*}\frac{dm^*(\mu_F)}{dE}\right]\left[\frac{1}{N}\frac{dn}{dm^*}\right]. \tag{9}$$

The nonlinearity is dominated by a change in the effective mass quantified by the non-parabolicity of dm^*/dE. The index curvature at the probe (typically near ENZ) indicates the sensitivity of the index to the

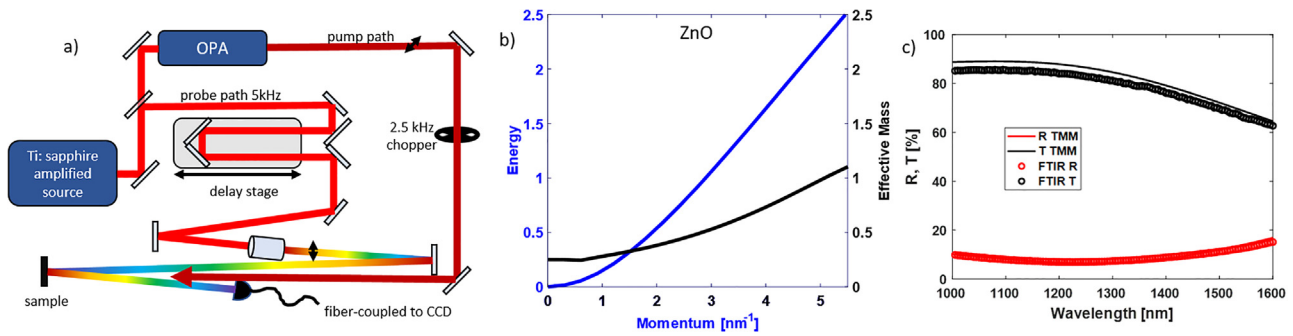

FIG. 1. (a) Experimental setup for nonlinear reflection measurements of GZO. (b) Energy–momentum diagram of ZnO near the Γ point toward A. (c) Transfer-matrix-method calculations for the GZO sample compared to the measured FTIR data for the GZO sample.

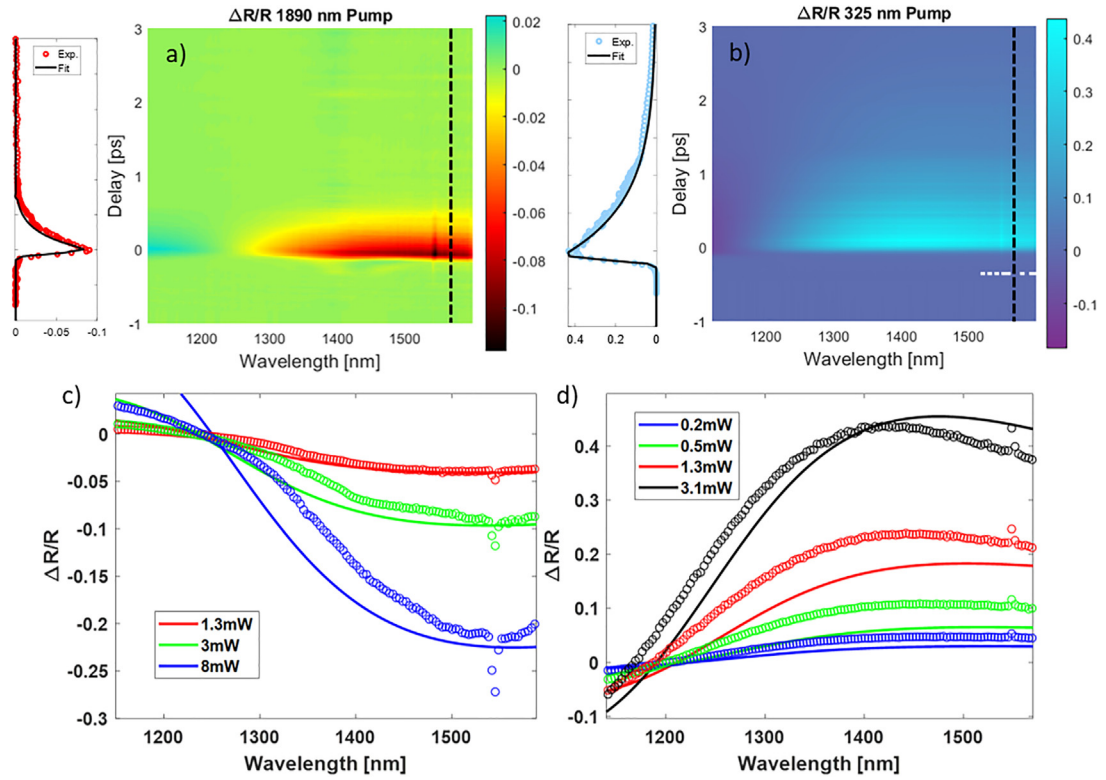

FIG. 2. (a) Surface plot of nonlinear reflection for a white light probe with wavelengths of 1120–1600 nm and a delay time of −1 to 3 ps (a) pumped with 3 mW at 1890 nm and (b) pumped with 3.1 mW at 325 nm. Cutlines taken at 1565 nm for each show the temporal dynamics of the film. Nonlinear reflection comparison of theory (solid) to experimental (dot) (c) pumped at 1890 nm with 1.3 (red), 3.3 (green), and 8.3 mW (blue) average power and (d) pumped at 325 nm with 0.2 (blue), 0.5 (green), 1.3 (red), and 3.1 mW (black) average power.

modification of the effective mass, quantified as dn/dm^*. A large number of carriers or high initial effective mass reduces the overall efficiency per unit energy.

Similarly, an interband FoM can be introduced considering the change in free carriers

$$FoM_{inter} = \left[\frac{A_{pump}}{E_g}\right]\left[\frac{1}{N}\frac{dN(\mu_F)}{dE}\right]\left[\frac{1}{m^*}\frac{-dn}{dN}\right]. \quad (10)$$

Here, the dn/dN describes the sensitivity of the index to a change in the carrier density (equivalent to a group velocity term) while dN/dE describes the number of available states near the Fermi energy. Many initial carriers or a high effective mass tend to decrease the efficiency per unit energy. Finally, the absorption is normalized by the bandgap energy, because the modulation of the carrier density is governed by $\Delta N \propto \frac{A}{\hbar\omega}$ with $\hbar\omega > E_g$. In essence, wide-bandgap materials require more energy to generate the same number of excess carriers.

From the FoM calculations, several important comparisons are made to predict the preferred film for various applications. GaN is found to be efficient for intraband operation due to its large non-parabolicity. At moderate energies, where other band structures are approximately hyperbolic, GaN forms a peak near the L-valley shown in Figs. 4(a)–4(c). This pushes the non-parabolicity to extreme levels as effective mass and DOS become quite large in this region, giving rise to a large modulation as seen in Figs. 3(a) and 3(b). However, realizing ENZ GaN in the telecom range (1.3–1.5 μm) is expected to be challenging as incremental blue-shifts in the plasma frequency via increased doping come with significant increases in the effective mass. On the other hand, doped CdO is found to be more efficient for interband. This is because CdO exhibits weak non-parabolicity and for low to moderately doped CdO, each excess electron, thus, induces a nearly equal change in the plasma frequency due to a slow variation in effective mass. Additionally, doped CdO has been shown to be ultra-low loss in the plasma frequency range of 2–5 μm, which leads to a sharp index dispersion in the ENZ region.[37,62,63] However, the high background permittivity requires many carriers to achieve ENZ, which reduces the energy efficiency.

For all-around materials, ITO and doped ZnO are well suited for both interband and intraband nonlinear processes. A moderate non-parabolicity and small background permittivity combine to induce efficient nonlinear effects in both interband and intraband operations. For interband operation, the low initial carrier concentration allows new carriers to contribute to a large percentage of the overall concentration without significantly increasing the average effective mass. For intraband operation, the initial effective mass is moderately low with non-parabolicity factor that allows for a large effective mass

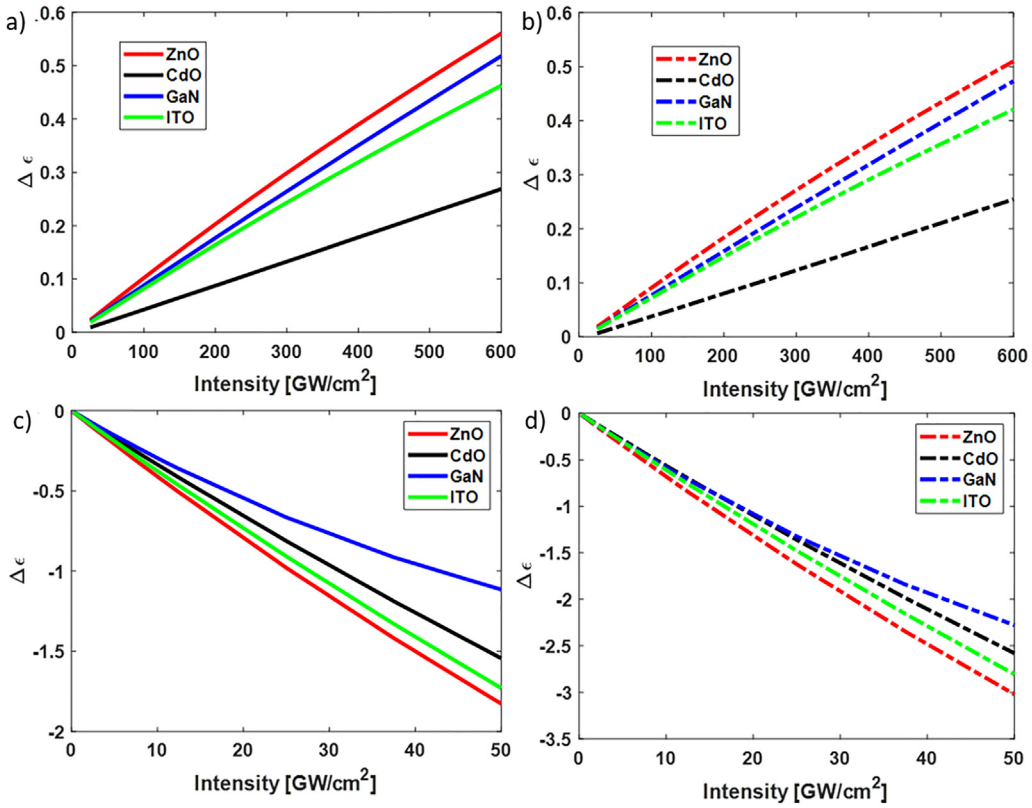

FIG. 3. (a) and (b) The change in permittivity for 100 nm thick films at ENZ calculated from intraband absorption at 787 nm for AZO, GaN, CdO, and ITO with $\lambda(\varepsilon' = 0) = 1.8\,\mu$m (solid, a) and $\lambda(\varepsilon' = 0) = 2.2\,\mu$m (dashed, b). (c) and (d) The change in permittivity calculated from interband absorption for 0.1 eV above the effective band edge of AZO, GaN, CdO, and ITO with $\lambda(\varepsilon' = 0) = 1.8\,\mu$m (solid, c) and $\lambda(\varepsilon' = 0) = 2.2\,\mu$m (dashed, d).

modulation. Additionally doped GaN, doped CdO, ITO, and doped ZnO (AZO/GZO) have been shown to achieve ENZ ranges as low as 1.2 μm.[12,17,28,52,64]

Additionally, the FoMs illustrate the tradeoffs in maximizing nonlinearities of ENZ materials, specifically the link between the absorptivity of the film for the pump and the need for a steep index dispersion at the probe. In the intraband case, this competition produces an optimum for most films in the range of $\varepsilon'' = 0.3$–0.6.[16] The interband nonlinearity, however, allows more freedom as the absorption of free carriers is not connected to the index slope near ENZ. As a result, one will always benefit from a lower loss at ENZ and higher losses at the pumping frequency with the limit arising due to impedance matching when the refractive index at ENZ approaches zero. A last note that while the interband is more efficient, it is generally slower than the intraband process, leading to a strength-bandwidth trade-off that should be considered for each application. Yet, both processes in TCOs have been shown to achieve THZ scale effects [see Figs. 2(a) and 2(b)].

In this work, we have developed a unifying and predictive *in silico* framework of nonlinear refraction in homogeneous thin ENZ films, requiring only a E–*k* band diagram and relevant experimental conditions. Collectively, this enables practical and rapid exploration and

TABLE I. Linear properties for AZO/GZO, GaN, CdO, and ITO used to evaluate the nonlinear response.

Material	Crossover wavelength (μm)	Carrier concentration ($\times 10^{20}$ cm^{-3})	Effective mass
AZO/GZO	1.8, 2.0, 2.2	3.94, 3.06. 2.44	0.35, 0.33, 0.32
GaN	1.8, 2.0, 2.2	6.88, 5.07, 3.90	0.38, 0.34, 0.32
CdO	1.8, 2.0, 2.2	7.68, 5.89, 4.63	0.41, 0.38, 0.37
ITO	1.8, 2.0, 2.2	4.44, 3.46, 2.77	0.39, 0.38, 0.37

TABLE II. HSE calculated lattice constants and bandgaps obtained by tuning the fraction of exact exchange α and the range separation parameter μ. The crystal structure of ZnO and GaN is wurtzite, that of CdO is the rock salt structure, and that of In_2O_3 is the bixbyite structure (space group 206, $Ia\bar{3}$), which is a body-centered cubic structure with eight formula units per primitive unit cell.

Material	α	μ (1/Å)	E_g (eV)	a (Å)
ZnO	0.3	0.0517	3.41	3.26
CdO	0.25	0.383	2.14	4.73
GaN	0.25	0.114	3.42	3.19
In_2O_3	0.25	0.147	2.68	5.11

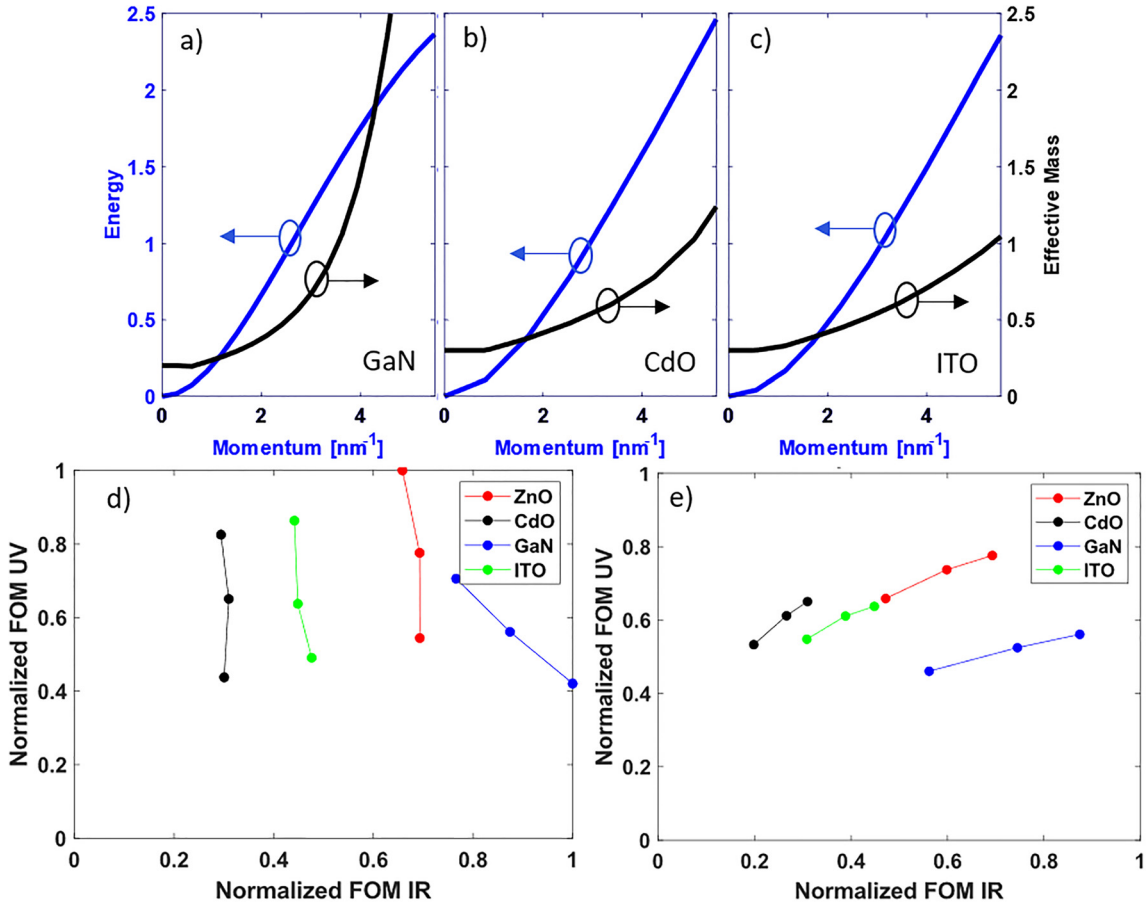

FIG. 4. (a)–(c) Energy–momentum and effective mass–momentum diagrams for GaN ($\Gamma \rightarrow A$), CdO ($\Gamma \rightarrow X$), and ITO ($\Gamma \rightarrow P$), respectively, calculated through using HSE. The effective mass is in the units of m^*/m_0. (d) and (e) Normalized figure of merit calculations for doped ZnO (AZO/GZO), GaN, CdO, and ITO. (d) fixes film loss ($\varepsilon''(\lambda_{ENZ}) = 0.7$) while varying ENZ wavelengths (1.8, 2.0, and 2.2 μm bottom to top), while (e) fixes the ENZ point to 2.0 μm and varying loss $\varepsilon'' = 0.3$, 0.5, and 0.7 (left to right).

optimization of unrealized ENZ materials for nonlinear optical applications. A FoM is also proposed for the interband interaction to aid in the intuitive understanding of performance tradeoffs and to compare with the intraband FoM. For example, doped GaN, doped CdO, ITO, and Al or Ga doped ZnO are investigated, wherein doped GaN is found to be the most efficient for intraband processes due to its highly non-parabolic structure while doped CdO is found to be the most efficient for interband processes due to its very parabolic band structure.

This work was supported by the Air Force Office of Scientific Research (Nos. FA9550-1-18-0151 and FA9550-16-10362).

The use of the Center for Nanoscale Materials, an Office of Science user facility, was supported by the U.S. Department of Energy, Office of Science, Office of Basic Energy Sciences under Contract No. DE-AC02-06CH11357.

We thank Dr. H. Morkoc for the help with the MBE growth of Ga-doped ZnO samples.

AUTHOR DECLARATIONS

Conflict of Interest

The authors have no conflicts to disclose.

Author Contributions

R.S. and A.B. contributed equally to this work.

DATA AVAILABILITY

The data that support the findings of this study are available from the corresponding author upon reasonable request.

REFERENCES

[1]D. Cotter, R. J. Manning, K. J. Blow, A. D. Ellis, A. E. Kelly, D. Nesset, I. D. Phillips, A. J. Poustie, and D. C. Rogers, "Nonlinear optics for high-speed digital information processing," Science **286**, 1523–1528 (1999).

[2]S. Basu, "A review of nonlinear optical organic materials," Ind. Eng. Chem. Prod. Res. Dev. **23**, 183–186 (1984).

[3]D. S. Chemla and J. Zyss, *Nonlinear Optical Properties of Organic Molecules and Crystals* (Academic Press, 1987).
[4]G. V. Naik, V. M. Shalaev, and A. Boltasseva, "Alternative plasmonic materials: Beyond gold and silver," Adv. Mater. **25**, 3264–3294 (2013).
[5]V. Kumar, "Linear and nonlinear optical properties of graphene: A review," J. Electron. Mater. **507**(50), 3773–3799 (2021).
[6]M. Z. Alam, S. A. Schulz, J. Upham, I. D. Leon, and R. W. Boyd, "Large optical nonlinearity of nanoantennas coupled to an epsilon-near-zero material," Nat. Photonics **12**, 79–83 (2018).
[7]D. De Ceglia, S. Campione, M. A. Vincenti, F. Capolino, and M. Scalora, "Low-damping epsilon-near-zero slabs: Nonlinear and nonlocal optical properties," Phys. Rev. B **87**, 155140 (2013).
[8]M. Pietrzyk, R. Kaipurath, D. Faccio, and A. D. Falco, "Epsilon near zero metamaterials ultra-low power nonlinear applications," in *Photonic and Phononic Properties of Engineered Nanostructures V* (International Society for Optics and Photonics, 2015), Vol. 9371, p. 93710Y.
[9]X. Li, M. Pietrzyk, D. Faccio, C. Rizza, A. Ciattoni, and A. D. Falco, "Linear and nonlinear optical behavior of epsilon near zero metamaterials: Opportunities and challenges," Proc. SPIE **10111**, 101111O (2017).
[10]D. Smirnova, D. Leykam, Y. Chong, and Y. Kivshar, "Nonlinear topological photonics," Appl. Phys. Rev. **7**, 021306 (2020).
[11]A. N. Poddubny, P. A. Belov, and Y. S. Kivshar, "Spontaneous radiation of a finite-size dipole emitter in hyperbolic media," Phys. Rev. A **84**, 023807 (2011).
[12]N. Kinsey, C. DeVault, A. Boltasseva, and V. M. Shalaev, "Near-zero-index materials for photonics," Nat. Rev. Mater. **4**, 742–760 (2019).
[13]O. Reshef, I. De Leon, M. Z. Alam, and R. W. Boyd, "Nonlinear optical effects in epsilon-near-zero media," Nat. Rev. Mater. **4**, 535–551 (2019).
[14]D. Fomra, K. Ding, V. Avrutin, Ü. Özgür, and N. Kinsey, "Al:ZnO as a platform for near-zero-index photonics: Enhancing the doping efficiency of atomic layer deposition," Opt. Mater. Express **10**, 3060 (2020).
[15]A. Capretti, Y. Wang, N. Engheta, and L. Dal Negro, "Comparative study of second-harmonic generation from epsilon-near-zero indium tin oxide and titanium nitride nanolayers excited in the near-infrared spectral range," ACS Photonics **2**, 1584–1591 (2015).
[16]R. Secondo, J. Khurgin, and N. Kinsey, "Absorptive loss and band non-parabolicity as a physical origin of large nonlinearity in epsilon-near-zero materials," Opt. Mater. Express **10**, 1545 (2020).
[17]L. Caspani, R. P. M. Kaipurath, M. Clerici, M. Ferrera, T. Roger, A. Di Falco, J. Kim, N. Kinsey, V. M. Shalaev, A. Boltasseva, and D. Faccio, "Enhanced nonlinear refractive index in epsilon-near-zero materials," Phys. Rev. Lett. **116**, 239901 (2016).
[18]R. M. Kaipurath, M. Pietrzyk, L. Caspani, T. Roger, M. Clerici, C. Rizza, A. Ciattoni, A. D. Falco, and D. Faccio, "Optically induced metal-to-dielectric transition in epsilon-near-zero metamaterials," Sci. Rep. **6**, 27700 (2016).
[19]I. Liberal and N. Engheta, "Near-zero refractive index photonics," Nat. Photonics **11**, 149–158 (2017).
[20]A. M. Mahmoud and N. Engheta, "Wave–matter interactions in epsilon-and-mu-near-zero structures," Nat. Commun. **5**, 5638 (2014).
[21]N. Kinsey and J. Khurgin, "Nonlinear epsilon-near-zero materials explained: Opinion," Opt. Mater. Express **9**, 2793 (2019).
[22]J. B. Khurgin, M. Clerici, and N. Kinsey, "Fast and slow nonlinearities in epsilon-near-zero materials," Laser Photonics Rev. **15**, 2000291 (2021).
[23]A. Ciattoni and E. Spinozzi, "Efficient second-harmonic generation in micrometer-thick slabs with indefinite permittivity," Phys. Rev. A **85**, 043806 (2012).
[24]M. A. Vincenti, D. De Ceglia, A. Ciattoni, and M. Scalora, "Singularity-driven second- and third-harmonic generation at ε-near-zero crossing points," Phys. Rev. A **84**, 063826 (2011).
[25]A. Ciattoni, C. Rizza, and E. Palange, "Extreme nonlinear electrodynamics in metamaterials with very small linear dielectric permittivity," Phys. Rev. A **81**, 043839 (2010).
[26]T. S. Luk, D. De Ceglia, S. Liu, G. A. Keeler, R. P. Prasankumar, M. A. Vincenti, M. Scalora, M. B. Sinclair, and S. Campione, "Enhanced third harmonic generation from the epsilon-near-zero modes of ultrathin films," Appl. Phys. Lett. **106**, 151103 (2015).
[27]S. Benis, N. Munera, R. Acuña, D. J. Hagan, and E. W. Van Stryland, "Nonlinear Fresnel coefficients due to giant ultrafast nonlinearities in indium tin oxide (conference presentation)," in *Ultrafast Phenomena and Nanophotonics XXIII*, edited by M. Betz and A. Y. Elezzabi (SPIE, 2019), Vol. 10916, p. 35.
[28]M. Clerici, N. Kinsey, C. DeVault, J. Kim, E. G. Carnemolla, L. Caspani, A. Shaltout, D. Faccio, V. Shalaev, A. Boltasseva, and M. Ferrera, "Controlling hybrid nonlinearities in transparent conducting oxides via two-colour excitation," Nat. Commun. **8**, 15829 (2017).
[29]J. Khurgin, M. Clerici, V. Bruno, L. Caspani, C. DeVault, J. Kim, A. Shaltout, A. Boltasseva, V. Shalaev, M. Ferrera, D. Faccio, and N. Kinsey, "Adiabatic frequency conversion in epsilon near zero materials: The role of group velocity," Optica **7**, 226–231 (2020).
[30]Y. Zhou, M. Z. Alam, M. Karimi, J. Upham, O. Reshef, C. Liu, A. E. Willner, and R. W. Boyd, "Broadband frequency translation through time refraction in an epsilon-near-zero material," Nat. Commun. **11**, 1–7 (2020).
[31]J. B. Khurgin, "Slow light in various media: A tutorial," Adv. Opt. Photonics **2**, 287 (2010).
[32]S. Benis, D. J. Hagan, and E. W. Van Stryland, "Enhancement mechanism of nonlinear optical response of transparent conductive oxides at epsilon-near-zero," in *Conference on Lasers and Electro-Optics* (OSA, 2018), p. FF2E.1.
[33]S. Benis, P. Zhao, D. J. Hagan, and E. W. Van Stryland, "Nondegenerate, transient nonlinear refraction of indium tin oxide excited at epsilon-near-zero," in *Nonlinear Optics* (OSA, 2017), p. NW1A.3.
[34]N. Kinsey, C. DeVault, J. Kim, M. Ferrera, V. M. Shalaev, and A. Boltasseva, "Epsilon-near-zero Al-doped ZnO for ultrafast switching at telecom wavelengths," Optica **2**, 616–622 (2015).
[35]S. Campione, D. De Ceglia, M. A. Vincenti, M. Scalora, and F. Capolino, "Electric field enhancement in epsilon-near slabs under TM-polarized oblique incidence," Phys. Rev. B **87**, 035120 (2013).
[36]C. Argyropoulos, G. D'Aguanno, and A. Alù, "Giant second-harmonic generation efficiency and ideal phase matching with a double ε-near-zero cross-slit metamaterial," Phys. Rev. B **89**, 235401 (2014).
[37]S. Saha, B. T. Diroll, J. Shank, Z. Kudyshev, A. Dutta, S. N. Chowdhury, T. S. Luk, S. Campione, R. D. Schaller, V. M. Shalaev, A. Boltasseva, and M. G. Wood, "Broadband, high-speed, and large-amplitude dynamic optical switching with yttrium-doped cadmium oxide," Adv. Funct. Mater. **30**, 1908377 (2020).
[38]X. Liu, J. Park, J. H. Kang, H. Yuan, Y. Cui, H. Y. Hwang, and M. L. Brongersma, "Quantification and impact of nonparabolicity of the conduction band of indium tin oxide on its plasmonic properties," Appl. Phys. Lett. **105**, 181117 (2014).
[39]L. D. Whalley, J. M. Frost, B. J. Morgan, and A. Walsh, "Impact of nonparabolic electronic band structure on the optical and transport properties of photovoltaic materials," Phys. Rev. B **99**, 085207 (2019).
[40]P. H. Jefferson, S. A. Hatfield, T. D. Veal, P. D. C. King, C. F. McConville, J. Zúñiga-Pérez, and V. Muñoz-Sanjosé, "Bandgap and effective mass of epitaxial cadmium oxide," Appl. Phys. Lett. **92**, 022101 (2008).
[41]F. Ruske, A. Pflug, V. Sittinger, B. Szyszka, D. Greiner, and B. Rech, "Optical modeling of free electron behavior in highly doped ZnO films," Thin Solid Films **518**, 1289–1293 (2009).
[42]B. T. Diroll, P. Guo, R. P. H. Chang, and R. D. Schaller, "Large transient optical modulation of epsilon-near-zero colloidal nanocrystals," ACS Nano **10**, 10099–10105 (2016).
[43]A. Ajay, J. Schörmann, M. Jiménez-Rodriguez, C. B. Lim, F. Walther, M. Rohnke, I. Mouton, L. Amichi, C. Bougerol, M. I. Den Hertog, M. Eickhoff, and E. Monroy, "Ge doping of GaN beyond the Mott transition," J. Phys. D. Appl. Phys. **49**, 445301 (2016).
[44]K. Ueno, Y. Arakawa, A. Kobayashi, J. Ohta, and H. Fujioka, "Highly conductive Ge-doped GaN epitaxial layers prepared by pulsed sputtering," Appl. Phys. Express **10**, 101002 (2017).
[45]A. E. Wickenden, L. B. Rowland, K. Doverspike, D. K. Gaskill, J. A. Freitas, D. S. Simons, and P. H. Chi, "Doping of gallium nitride using disilane," J. Electron. Mater. **24**, 1547–1550 (1995).
[46]E. Sachet, C. T. Shelton, J. S. Harris, B. E. Gaddy, D. L. Irving, S. Curtarolo, B. F. Donovan, P. E. Hopkins, P. A. Sharma, A. L. Sharma, J. Ihlefeld, S. Franzen, and J. P. Maria, "Dysprosium-doped cadmium oxide as a gateway material for mid-infrared plasmonics," Nat. Mater. **14**, 414–420 (2015).

[47]E. L. Runnerstrom, K. P. Kelley, E. Sachet, C. T. Shelton, and J. P. Maria, "Epsilon-near-zero modes and surface plasmon resonance in fluorine-doped cadmium oxide thin films," ACS Photonics **4**, 1885–1892 (2017).
[48]A. Cleri, J. Tomko, K. Quiambao-Tomko, M. V. Imperatore, Y. Zhu, J. R. Nolen, J. Nordlander, J. D. Caldwell, Z. Mao, N. C. Giebink, K. P. Kelley, E. L. Runnerstrom, P. E. Hopkins, and J. P. Maria, "Mid-wave to near-IR optoelectronic properties and epsilon-near-zero behavior in indium-doped cadmium oxide," Phys. Rev. Mater. **5**, 35202 (2021).
[49]P. Yeh, *Optical Waves in Layered Media (Pure & Applied Optics)* (Wiley-Blackwell, 1988).
[50]S. Dal Forno and J. Lischner, "Electron-phonon coupling and hot electron thermalization in titanium nitride," Phys. Rev. Mater. **3**, 1–8 (2019).
[51]J. R. M. Saavedra, A. Asenjo-Garcia, and F. J. García De Abajo, "Hot-electron dynamics and thermalization in small metallic nanoparticles," ACS Photonics **3**, 1637–1646 (2016).
[52]V. Ortiz, J. Nagle, and A. Alexandrou, "Influence of the hole population on the transient reflectivity signal of annealed low-temperature-grown GaAs," Appl. Phys. Lett. **80**, 2505–2507 (2002).
[53]M. Z. Alam, M. Z. Alam, I. D. Leon, and R. W. Boyd, "Large optical nonlinearity of indium tin oxide in its epsilon-near-zero region," Science **352**, 795–795 (2016).
[54]H. Y. Liu, V. Avrutin, N. Izyumskaya, Ü. Özgür, A. B. Yankovich, A. V. Kvit, P. M. Voyles, and H. Morkoç, "Electron scattering mechanisms in GZO films grown on a-sapphire substrates by plasma-enhanced molecular beam epitaxy," J. Appl. Phys. **111**, 103713 (2012).
[55]H. Y. Liu, V. Avrutin, N. Izyumskaya, M. A. Reshchikov, Ü. Özgür, and H. Morkoç, "Highly conductive and optically transparent GZO films grown under metal-rich conditions by plasma assisted MBE," Phys. Status Solidi—Rapid Res. Lett. **4**, 70–72 (2010).
[56]D. O. Demchenko, B. Earles, H. Y. Liu, V. Avrutin, N. Izyumskaya, Ü. Özgür, and H. Morkoç, "Impurity complexes and conductivity of Ga-doped ZnO," Phys. Rev. B **84**, 075201 (2011).
[57]R. Secondo, D. Fomra, N. Izyumskaya, V. Avrutin, J. N. Hilfiker, A. Martin, Ü. Özgür, and N. Kinsey, "Reliable modeling of ultrathin alternative plasmonic materials using spectroscopic ellipsometry [Invited]," Opt. Mater. Express **9**, 760 (2019).
[58]J. Paul, J. K. Wahlstrand, M. Miscuglio, V. J. Sorger, and Y. Gui, "Two-beam coupling by a hot electron nonlinearity," Opt. Lett. **46**(2), 428–431 (2021).
[59]J. Heyd, G. E. Scuseria, and M. Ernzerhof, "Hybrid functionals based on a screened Coulomb potential," J. Chem. Phys. **118**, 8207 (2003).
[60]G. Kresse and J. Furthmüller, "Efficiency of ab-initio total energy calculations for metals and semiconductors using a plane-wave basis set," Comput. Mater. Sci. **6**, 15–50 (1996).
[61]Y.-S. Kim, M. Marsman, G. Kresse, F. Tran, and P. Blaha, "Towards efficient band structure and effective mass calculations for III-V direct band-gap semiconductors," Phys. Rev. B **82**, 205212 (2010).
[62]A. Wang, J. R. Babcock, N. L. Edleman, A. W. Metz, M. A. Lane, R. Asahi, V. P. Dravid, C. R. Kannewurf, A. J. Freeman, and T. J. Marks, "Indium-cadmium-oxide films having exceptional electrical conductivity and optical transparency: Clues for optimizing transparent conductors," Proc. Natl. Acad. Sci. U. S. A. **98**, 7113–7116 (2001).
[63]S. K. Vasheghani Farahani, T. D. Veal, P. D. C. King, J. Ziga-Pérez, V. Muoz-Sanjosé, and C. F. McConville, "Electron mobility in CdO films," J. Appl. Phys. **109**, 073712 (2011).
[64]Y. Wang, A. Capretti, and L. Dal Negro, "Wide tuning of the optical and structural properties of alternative plasmonic materials," Opt. Mater. Express **5**, 2415 (2015).